Int. J. Heat Mass Transfer. Vol. 19, pp. 613–624. Pergamon Press 1976. Printed in Great Britain

TURBULENT MASS TRANSFER AT FREE, GAS–LIQUID INTERFACES, WITH APPLICATIONS TO OPEN-CHANNEL, BUBBLE AND JET FLOWS

T. G. THEOFANOUS, R. N. HOUZE and L. K. BRUMFIELD
Purdue University, West Lafayette, IN 47907, U.S.A.

(*Received* 12 *July* 1974 *and in revised form* 2 *April* 1975)

Abstract—Gas absorption by a turbulent liquid in the absence of external (gas-imposed) interfacial shear is discussed. The primary tool used is dimensional analysis. Two distinct mass-transfer regimes, associated with energy-containing and energy-dissipating turbulent motions, are identified. Relationships are obtained for each regime, and a criterion, based on the turbulence Reynolds number, is determined for the applicability of each. The mass-transfer model is evaluated for four flow situations for which turbulence data are either available or can be estimated (open-channel flow with and without grid-produced turbulence, bubble flow, and jet flow).

NOMENCLATURE

c, solute concentration;
c_b, bulk concentration;
c_s, interfacial concentration;
C_{IMA}, constant of $k_L = k_L^I$ regime, equation (9);
C_L, constant of Levich model;
C_{LE}, constant of large-eddy model;
C_{SE}, constant of small-eddy model;
C_{UET}, constant of $k_L = k_L^D$ regime, equation (7);
D, molecular diffusivity;
d, pipe diameter;
d_B, bubble diameter;
E, average percent error;
$F(\alpha)$, factor for transient effects;
j, absorption flux;
k_L, overall mass-transfer coefficient;
k_L^D, mass-transfer coefficient for dissipative regime;
k_L^I, mass-transfer coefficient for inertial regime;
L, macroscale;
L_S, length of mass-transfer section;
l_K, Kolmogoroff length scale;
M, mesh size;
R, radius of protuberances on jet surface;
Re, flow Reynolds number;
Re_t, turbulence Reynolds number, LV/ν;
Re_t^*, critical turbulence Reynolds number;
S, sensitivity parameter;
Sc, Schmidt number;
Sh, Sherwood number;
T, characteristic time of large-scale motions, $L/V\sqrt{2}$;
t, time;
t^*, time of duration of the initial period of decay;
t_{exp}, exposure time for mass transfer;
V, turbulence intensity;
$\bar{V}$, bulk velocity;
V_0, Levich's characteristic eddy velocity;
V_s, relative velocity between bubble and liquid or surface velocity;
V_*, shear velocity;
v_K, Kolmogoroff velocity scale;
x, y, Cartesian coordinates, x in direction of mean flow;
x^*, length of duration of the initial period of decay;
x_0, distance of mass-transfer section from grid;
We_t, turbulence Weber number, $V\sqrt{(\rho L/\sigma)}$.

Greek symbols

α, t_{exp}/T;
β, parameter in unsteady transfer analysis, equation (B.1);
δ, penetration thickness;
ε, rate of viscous dissipation per unit mass;
λ, microscale;
π, 3.14159....;
ρ, density;
σ, surface tension;
ν, kinematic viscosity.

1. INTRODUCTION

THE PROBLEM considered in this paper is the theoretical prediction of mass-transfer coefficients for gas absorption by turbulent liquids. In terms of practical geometries, a large number of possibilities exist. Mass transfer data are now available for open-channel flows, bubble flows, jet flows, and film flows. From a fundamental viewpoint, the classical problem of turbulence interaction with a "free" gas–liquid interface and the implications for mass transfer should be common to all. On the other hand, differences in the "structure" and "property range" of turbulence would be expected. By focusing on individual flow regimes, previous work has implicitly emphasized these differences. The primary motivation for this study is to exploit the similarities, instead. The feasibility of a unified approach is thus explored. Open-channel flows, bubble (pipe) flows, and jet flows are considered in this paper. Film flows are discussed elsewhere [1].

2. PREVIOUS WORK

The role of surface tension in affecting the fluid motions within the "interfacial region" and, hence, the mass-transfer rates, remains uncertain. Two widely different, but yet partially successful, approaches exist. The first, due to Levich [2], is based on the concept of a surface-tension-damped laminar sublayer. The second, due to Fortescue and Pearson [3] and Lamont and Scott [4], is based on idealized eddy structures of turbulence unaffected by interfacial forces. These eddy models, themselves, are in difference. Fortescue and Pearson's "large-eddy" model assumes that the energy-containing motions control the transfer process. Lamont and Scott's "small-eddy" model assumes that the dissipating motions are controlling. The equations for these three models are shown in Table 1. According to Levich, the characteristic eddy velocity, V_0, which is identified with the shear velocity, V_*, is utilized to characterize the mass-transfer properties of the interface. For the "small-eddy" model, the rate of dissipation, ε, is needed instead. According to the "large-eddy" model, the turbulence intensity, V, and macroscale, L, are the relevant turbulence properties. The published recommendations for the proportionality constants are also shown in Table 1. These values were "calculated" from the detailed physical models postulated in each case. Only the constant suggested by Levich was given as an order-of-magnitude estimate. The various model-data combinations previously examined in the literature are indicated in Table 2. Details on these applications and the quantitative aspects of the comparisons are deferred until a latter portion of this paper.

Table 1. Comparison of mass-transfer models

	Data set				
Theory	Open-channel flow Brown [7]	Bubble flow Lamont and Scott [4, 8, 9]	Open-channel flow with grids Fortescue and Pearson [3, 10]	Water jets Davies and Ting [11, 12]	Kerosene jets Davies and Hameed [13, 14]
Levich $k_L = C_L(D\rho V_0^3/\sigma)^{1/2}$ $C_L = 0.32$ Davies [25] $C_L \sim O(1)$ Levich [2]	with $V_0 = V_*$ $C_L = 1.6$ $E = 18\%$ $S = 0.81$	with $V_0 = V_*$ $C_L = 3.2$ $E = 48\%$ $S = 1.7$	with $V_0 = V$ $C_L = 88$ $E = 33\%$ $S = 2.4$	with $V_0 = V_*$ $C_L = 0.32$ $E = 15\%$ $S = 0.81$	with $V_0 = V_*$ $C_L = 0.20$ $E = 24\%$ $S = 0.67$
Small-eddy $k_L = C_{SE}(\sqrt{D})(\varepsilon/\nu)^{1/4}$ $C_{SE} = 0.4$ Lamont and Scott [4] $C_{SE} = 0.196$ Prasher [23]	with $\varepsilon = V^3/L$ $C_{SE} = 0.22$ $E = 15\%$ $S = 0.48$	with $\varepsilon = V^3/L$ $C_{SE} = 0.30$ $E = 16\%$ $S = 1.2$	with $\varepsilon = -\frac{3}{2}\frac{dV^2}{dt}$ $C_{SE} = 0.56$ $E = 11\%$ $S = 1.4$	with $\varepsilon = -\frac{3}{2}\frac{dV^2}{dt}$ $C_{SE} = 0.24$ $E = 23\%$ $S = 0.63$	with $\varepsilon = -\frac{3}{2}\frac{dV^2}{dt}$ $C_{SE} = 0.34$ $E = 39\%$ $S = 0.54$
Large-eddy $k_L = C_{LE}\sqrt{(DV/L)}$ $C_{LE} = 1.07$ Brown [7] $C_{LE} = 1.46$ Fortescue and Pearson [3]	$C_{LE} = 1.0$ $E = 22\%$ $S = 0.02$	$C_{LE} = 0.64$ $E = 13\%$ $S = 0.98$	$C_{LE} = 1.1$ $E = 4\%$ $S = 0.82$	$C_{LE} = 0.55$ $E = 25\%$ $S = 0.59$	$C_{LE} = 0.73$ $E = 40\%$ $S = 0.52$
Present model Equations (7) and (9)	$C_{UET} = 0.25$ $C_{IMA} = 0.73$ $E = 10\%$ $S = 0.81$	$C_{IMA} = 0.63$ $E = 11\%$ $S = 0.97$	$C_{IMA} = 0.85$ $E = 4\%$ $S = 0.92$	$C_{IMA} = 0.50$ $E = 26\%$ $S = 0.58$	$C_{IMA} = 0.66$ $E = 41\%$ $S = 0.51$

Table 2. Model-data combinations previously examined

	Data set					
Theory	Open-channel flow Bieber [22]	Open-channel flow Brown [7]	Bubble flow Lamont and Scott [4]	Open-channel flow with grids Fortescue and Pearson [3]	Water jets Davies and Ting [11]	Kerosene jets Davies and Hameed [13]
Levich	X	X	X	X	[11]	[13]
Small-eddy	[23]	X	[4]	[4]	X	X
Large-eddy	X	[7]	X	[3]	X	X

3. ANALYSIS

The essential difficulty in the "eddy" models is with the arbitrary and conflicting assumptions regarding the group of motions controlling the transfer process. The principal goal of this section is to reconsider these differences by deducing the range of applicability for each model. Dimensional analysis is utilized to recover the "small-eddy" and "large-eddy" results and to incorporate transient (entrance) effects in the formulation. In this manner, the proportionality constants are not tied to a specific, postulated, flow microstructure. Instead, they are determined from the experimental data in an optimal fashion. Since the uniformity of these constants among different physical flow systems provides a measure of the success of the sought fundamental model, spurious differences are eliminated by a consistent estimation of turbulence properties and an explicit accounting for entrance effects.

The magnitude of the turbulence Reynolds number, based on intensity and macroscale, provides a measure of the degree of independence between the "large-scale", energy-containing motions and the "small-scale", dissipative ones. For $Re_t = LV/\nu \gg 1$, the equilibrium range exists, and its statistical behavior is determined [5] solely by the rate of dissipation per unit mass, ε, and the kinematic viscosity, ν. These physical parameters provide the natural length and velocity scales in this range:

$$v_K = (\nu\varepsilon)^{1/4} \text{ and } l_K = \left(\frac{\nu^3}{\varepsilon}\right)^{1/4}. \tag{1}$$

The dissipation rate may be expressed in terms of the characteristic length and velocity scales of the energy-containing motions through the empirical formula [6]:

$$\varepsilon = \frac{V^3}{L} \tag{2}$$

where V is the turbulence intensity and L is the macroscale of turbulence. From these relations the scale "separation" between the two groups of motions may be obtained as:

$$\frac{l_K}{L} = Re_t^{-3/4}. \tag{3}$$

Similarly, the "separation" between the characteristic times of the large-scale and small-scale motions (L/V and l_K/v_K, respectively) is given by:

$$\frac{L/V}{l_K/v_K} = Re_t^{1/2}. \tag{4}$$

Assuming, as was done in the turbulence-centered eddy models, that the turbulence–interface hydrodynamic interaction is "similar" for both groups of motions, the following deductions may be made:

(a) The high Schmidt number mass-transfer process is also "similar" for both groups of motions. More specifically, the small-penetration (as compared to the scale of the motion) character of the energy-containing eddies is also found in the small, dissipative motions:

$$\frac{\delta}{l_K} \simeq 4Sc^{-1/2}. \tag{5}$$

(b) The characteristic times L/V and l_K/v_K may also be viewed as effective renewal times for the motions in the vicinity of the interface. Equation (4) then indicates that for $Re_t \gg 1$, the small-scale motions are by far more effective in transferring mass across the interfacial region than the large-scale ones. Hence, for $Re_t \gg 1, k_L = k_L^D$ where k_L^D is the mass-transfer coefficient determined from the small-scale motions alone. When the condition $Re_t \gg 1$ is *not* satisfied, the universal equilibrium range is not developed, and $k_L = k_L^I$ where k_L^I is the mass-transfer coefficient determined from the energy-containing motions alone.

(c) In the k_L^I regime, entrance effects are determined from the ratio of the exposure time for mass transfer, t_{exp}, and the characteristic time of the large-scale motions, L/V. When this ratio is much larger than one, entrance effects are negligible. In the k_L^D regime, interaction effects with the large-scale motions may be viewed as "entrance" effects for the small-scales. The large scales convect the small scales without appreciably distorting them as seen from equation (3) for $Re_t \gg 1$. Small scales brought up to the interface experience an exposure time of L/V and their characteristic time is l_K/v_K. As may be seen from equation (4) this ratio is $Re_t^{1/2} \gg 1$, and interaction effects are negligible in this regime.

For the $Re_t \gg 1$ mass-transfer regime, k_L^D should depend only on the local viscous dissipation rate per unit mass, ε, kinematic viscosity, ν, and molecular diffusivity, D. Dimensional analysis yields:

$$\frac{k_L^D}{(\varepsilon\nu)^{1/4}} \propto f\left(\frac{\nu}{D}\right). \tag{6}$$

Experimental and theoretical studies concur that for high Schmidt number processes at zero-shear interfaces, $k_L \propto D^{1/2}$. Thus:

$$k_L = k_L^D = C_{UET} D^{1/2}\left(\frac{\varepsilon}{\nu}\right)^{1/4} \text{ for } Re_t \gg 1. \tag{7}$$

For ease in reference, we designate this result as "UET" (Universal Equilibrium Theory). The constant of proportionality, C_{UET}, is a universal constant independent of the particular geometry and other macroscopic variables of the system.

For the low-Re_t mass-transfer regime, k_L^I should depend on the length and velocity scales of the energy-containing motions, L and V, the molecular diffusivity, D, and t_{exp}, which characterizes the entrance effects. Dimensional analysis yields:

$$\frac{k_L^I L}{D} \propto f\left(\frac{LV}{D}, \frac{t_{exp}}{L/V}\right). \tag{8}$$

Requiring $k_L^I \propto D^{1/2}$ as before:

$$k_L = k_L^I = C_{IMA} F(\alpha)\left(\frac{DV}{L}\right)^{1/2} \text{ for } Re_t \text{ not} \gg 1 \tag{9}$$

with

$$\alpha = \frac{2^{1/2} t_{exp}}{L/V}. \tag{10}$$

For ease of reference, this result is termed "IMA" (Inertial Motion Approximation). The constant, C_{IMA}, is *not* expected to be universal due to greater sensitivity of the large-scale motions to macroscopic flow details. It is hoped, however, that it will prove to be only weakly dependent on the shape of the energy spectrum at small wavenumbers. The function $F(\alpha)$ decreases monotonically and approaches 1 asymptotically as $\alpha \to \infty$. An estimate of this function is provided by recourse to a specific eddy model. The derivation for steady turbulence conditions is given in Appendix A. The more general case for time-varying length and velocity scales is presented in Appendix B.

Since the ranges of applicability of the IMA and the UET are related to the magnitude of Re_t, there is an intermediate range of Re_t for which these asymptotic results are not precise. An *order-of-magnitude* estimate of this transition region may be obtained by extending these asymptotic results to obtain an abrupt transition. This transition Re_t-value is denoted by Re_t^* and is estimated by

$$Re_t^* = \left(\frac{C_{IMA}}{C_{UET}}\right)^4. \tag{11}$$

With the values of the constants determined in the next section, this value of Re_t^* is in the range of a *few hundred*. This would imply an order-of-magnitude separation in the characteristic times, and two orders-of-magnitude separation in the scales, between the energy-containing and dissipative motions.

The possibly strong directional structure of turbulence was not included in the above formulation. The principal difficulty that arises is with regard to the "appropriate" choice of L and V and its implication for the constants C_{UET} and C_{IMA}. For the IMA, the choice of L and V in the direction of the mean flow appears appropriate, and it should be expected that a different partition of turbulence energy (as might be dictated by the detailed dynamics of the flow system) would be reflected as small variations in the values of C_{IMA}. The same choice, however, for the UET would commonly lead to an overestimation of the dissipation rate [as calculated by equation (2)], and, hence, would yield an underestimation of C_{UET} as compared to its true universal value. A "mean" intensity averaged over all three directions would represent an improvement. The sensitivity to the accuracy of L is only minimal. However, the true *local* (in the vicinity of the interface) dissipation rate should be utilized when available.

4. APPLICATIONS

Evaluation of the model depends on the accuracy with which the quantities L and V are known or can be predicted. Brown's [7] work represents the only mass-transfer study with simultaneous measurements of the hydrodynamic quantities L and V. Since turbulence in pipe flow has been studied extensively, the L's and V's for the mass-transfer data of Lamont and Scott [4, 8, 9] for discrete, widely-separated bubbles transported in turbulent pipe flow may also be considered known with confidence. These two sets of data will be employed to evaluate the transition criterion, Re_t^*, and the constants in equations (7) and (9). Two flow systems will then be considered for which the requisite turbulence characteristics are not known and must be estimated. These are the data of Fortescue and Pearson [3, 10] for decaying turbulent flow behind a grid in an open channel and those of Davies and coworkers [11–14] for turbulent water and kerosene jets. The comparisons are presented separately for each one of the cases considered in terms of the "predicted" vs "measured" mass-transfer coefficient.

4.1. *Systems with known turbulence characteristics*

For reference, the most important characteristics of these experiments are presented in Table 3. The turbulence Reynolds numbers obtained in Brown's experiments with open-channel flow are very large and extend well above the previously-suggested value for Re_t^* of a few hundred. The values of Re_t in the experiments of Lamont and Scott, on the other hand, are well below this criterion for transition.

Table 3. Important characteristics of mass-transfer experiments with known turbulence properties

Experimental conditions	Brown [7]	Lamont and Scott [4, 8, 9]
Description of flow	Open-channel flow	Bubble flow
Absorbing system	O_2–water	CO_2–water
Characteristics of physical system	Channel width: 6 in Water depth: 3 and 6 in	Pipe diameter: $\frac{5}{16}$ and $\frac{3}{8}$ in Flow orientations: horizontal and vertical
Type of turbulence	Shear-generated and steady	Shear-generated and steady
Range of flow Reynolds number	$46\,400 \leqslant \frac{4R_H\bar{V}}{\nu} \leqslant 92\,800$ R_H = hydraulic radius	1810–22 400
Range of turbulence Reynolds number, Re_t	128–3940	4.25–38.4
Range of k_L, (cm/s)	3.4×10^{-3} to 7.3×10^{-3}	1.0×10^{-2} to 7.4×10^{-2}

4.1.1. *Open-channel flow.* The experimental measurements of Brown [7] were carried out in a small flume equipped to recirculate the flow. Experimental variables included the depth of the flow, velocity, bottom roughness, water temperature, and the surface area exposed to the solute gas. Brown accounted for the spatial variation in the turbulent nature of the flow in the channel by dividing, conceptually, the surface area into compartments. In the center of each compartment the instantaneous longitudinal velocity near the free surface was measured and recorded, and the macroscale and the turbulence intensity were then calculated. These quantities were utilized as the L and V in this application. Assuming $Re_t^* = 500$, Brown's mass-transfer data were predicted according to the present model by calculating the local k_L's (for each one of the compartments). If the local $Re_t > Re_t^*$, k_L was calculated from equation (7); if the local $Re_t < Re_t^*$, k_L was calculated from equation (9). The local k_L values were then area-averaged, and the best values of $C_{UET} = 0.25$ and $C_{IMA} = 0.73$ were determined by minimizing the sum of the squares of the deviations between the measured and predicted mass-transfer coefficients. In carrying out the calculations based on equation (9), it was found that transient absorption was confined to the compartments nearest the entrance of the channel. In evaluating α's for these compartments, t_{exp} is given by the length of a compartment divided by the average surface velocity of the liquid within the region. Predicted increases in the local mass-transfer coefficients due to transient absorption for compartments nearest the entrance of the channel (having $Re_t \leqslant Re_t^*$) are of the order of 30%; but the total surface-area fraction of these compartments is small, thereby resulting in an inconsequential increase in the overall k_L.

A measure of the sensitivity of a particular mass-transfer model to the parameters governing the mass-transfer process is provided by the slope of the "least-squares" line through the points on a plot of the predicted vs measured mass-transfer coefficient. This sensitivity parameter, denoted by S, has a value of 0.81 for the results shown in Fig. 2. It is informative to note the effect of varying Re_t^* on the calculated values of S. If one assumes $Re_t^* = 0$ (all mass transfer governed by the UET), $S = 0.48$. S increases to an essentially constant value of about 0.8 for $300 \leqslant Re_t^* \leqslant 700$. Assuming $Re_t^* = 1000$ gives $S = 0.48$, and for $Re_t^* = \infty$ (equivalent to assuming all mass transfer governed by the IMA), $S = 0.02$, similar to that for the large-eddy model. This lack of sensitivity is graphically shown in Fig. 3. The average error in the predictions from the present model remains at about 10% for $300 \leqslant Re_t^* \leqslant 700$ and increases for Re_t^* outside this range. These considerations provide an experimental determination of the range of the parameter, Re_t^*, which is in excellent agreement with the range deduced previously.

4.1.2. *Bubble flow.* The investigation of Lamont and Scott [4, 8, 9] considered the absorption of gas from bubbles transported in turbulent pipe flow of water for

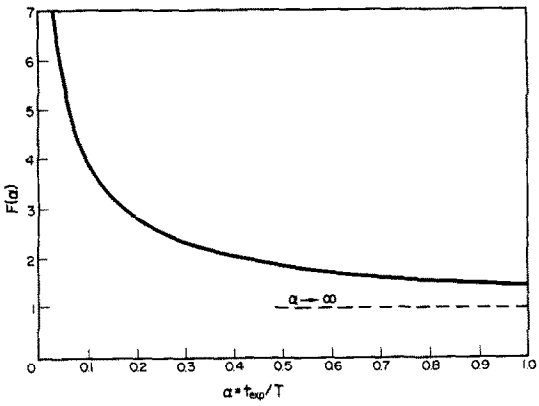

FIG. 1. The function $F(\alpha)$ as defined in equation (A.6).

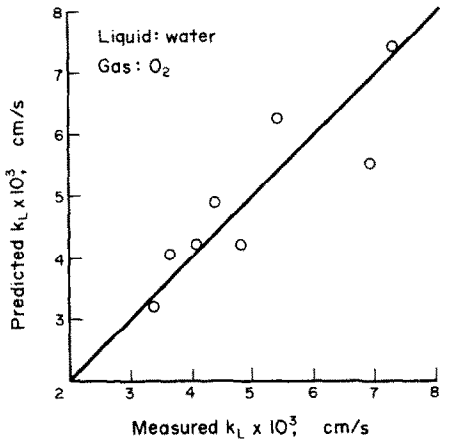

FIG. 2. Comparison of the results of the present model (with $C_{UET} = 0.25$, $C_{IMA} = 0.73$, $Re_t^* = 500$) with the data of Brown [7].

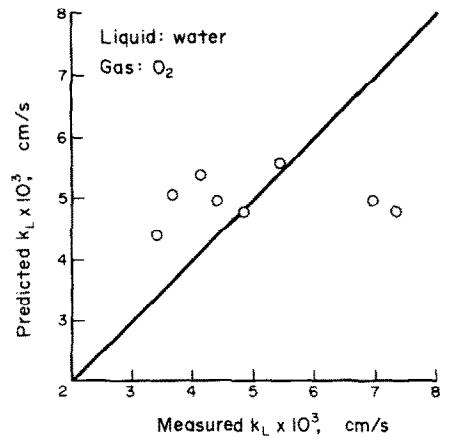

FIG. 3. Comparison of the results of the large-eddy model (with $C_{LE} = 1.0$) with the data of Brown [7].

both horizontal and vertical orientations. For the range of Reynolds numbers of Lamont and Scott's investigation, the integral length scale of turbulence, L, in the central region of the pipe is known [15] to be about $0.03d$, where d is the pipe diameter. The turbulence intensity, V, in the core of the pipe is known [16] to be approximately equal to the shear velocity (from the Blasius relation, $V_* = 0.2\nu Re^{7/8}/d$). From

Table 3, the Re_t values for this physical situation indicate that the energy-containing motions, *not* the energy-dissipating motions, should control the gas absorption rates. This explains why the result based on Lamont and Scott's "small-eddy" model, $k_L \propto Re^{0.69}$, is in disagreement with the experimental data, represented by $k_L \propto Re^{0.52}$. To evaluate the transient effects for the prediction of k_L by the present theory, t_{exp} is calculated as d_B/V_s, where d_B is the bubble diameter and V_s is the relative velocity between the bubble and the liquid in the core of the pipe. Bubble diameters ranged from about 0.3 to 0.7 of the pipe diameter, and in the calculations, a value of $d_B/d = 0.5$ was used. For the horizontal bubble flow [9] the ratio of the bubble velocity to the velocity of the total volumetric flow ranged from approximately 0.95 for small bubbles ($d_B/d = 0.36$) at $Re = 1400$ to 1.18 for large bubbles ($d_B/d = 0.65$) at $Re = 26000$. It can be shown that, for the horizontal flow conditions employed by Lamont and Scott, the transient effects on k_L are insignificant. This is not the case for the vertical orientations. For this case V_s was taken to be the wall-free terminal velocity of the bubble, as calculated according to Peebles and Garber [17]. This approach is consistent with the results of Baker and Chao [18], who found the bubble relative velocity in a turbulent water stream to be similar to the rise velocity of single bubbles through a quiescent liquid. Values of $F(\alpha)$ calculated from Lamont and Scott's vertical flow conditions range from 1.04 to 1.49.

The results of the present model are compared with the experimental data in Fig. 4. The best value for C_{IMA} was found to be 0.63. The sensitivity parameter, S, is 0.97, and the average error is 11%, indicating good agreement between prediction and experiment.

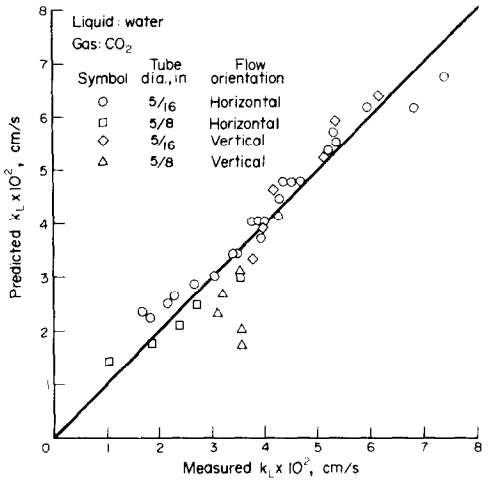

FIG. 4. Comparison of the results of the present model (with $C_{IMA} = 0.63$) with the data of Lamont and Scott [4, 8, 9].

4.2. *Systems with unknown turbulence characteristics*

For reference, the most important characteristics of these experiments are presented in Table 4. The turbulence Reynolds numbers for both Fortescue and Pearson's grid flow and the jet data of Davies and coworkers are low, indicating that the large-scale motions should control the transfer process. In these systems, the turbulence macroscales and intensities are not known but may be estimated by employing the concepts of decaying turbulence.

4.2.1. *Open-channel, grid-produced turbulent flow.* Fortescue and Pearson [3, 10] measured CO_2 absorption rates in decaying, turbulent water flow downstream of a grid in an open channel. For this flow system the turbulence properties are a function of position over the absorbing surface. In Appendix B, it is shown how the local stagnation-flow gas absorption flux, $j(t;\beta)$, may be utilized to incorporate transient effects for this more general situation. The proportionality constants in this derivation are chosen so that the result equals that for the IMA, equation (9), for the case of steady-state mass transfer in a flow with a uniform distribution of turbulence properties. The final result for the average mass-transfer coefficient is

$$k_L = \frac{2^{1/4} C_{IMA}}{(c_s - c_b) t_{exp}} \times \int_0^{t_{exp}} 1/2\{j(t;\beta = 1) + j(t;\beta = -1)\}\, dt. \quad (12)$$

Table 4. Important characteristics of mass-transfer experiments with estimated turbulence properties

Experimental conditions	Fortescue and Pearson [3, 10]	Davies and Ting [11, 12]	Davies and Hameed [13, 14]
Description of flow	Decaying flow downstream of a grid in an open channel	Liquid jet exiting into gas	
Absorbing system	CO_2–water	CO_2– and H_2–water	CO_2–, H_2– and He–kerosene
Characteristics of physical system	Channel width: 1 ft Channel length: 2 ft, 3 in Water depth: 1.5–2.0 in Mesh size: 5/16–5/8 in x_0 = 10 and 18 cm	Nozzle diameters: 0.102, 0.132, 0.1512 and 0.162 cm	Nozzle diameters: 0.130, 0.1296 and 0.162 cm
Type of turbulence	Grid-generated and decaying	Shear-generated and decaying	
Range of turbulence Reynolds number, Re_t	2.3–113	3.9–37	1.8–20
Range of k_L (cm/s)	1.3×10^{-3} to 2.7×10^{-3}	2.3×10^{-2} to 1.7×10^{-1}	2.5×10^{-2} to 4.9×10^{-1}

Expressions for the $j(t;\beta)$ are derived in Appendix C. In these experiments the water level in the test section was maintained at 1.5 to 2.0 in. A mean value of 1.75 in was utilized in all computations. Transient absorption is evaluated with $V_s = 1.2\,\bar{V}$, and its contribution is found to be about 25% of the total mass transfer.

The comparison of these results with the experimental data is given in Fig. 5. The best value of C_{IMA} for these data is 0.85.

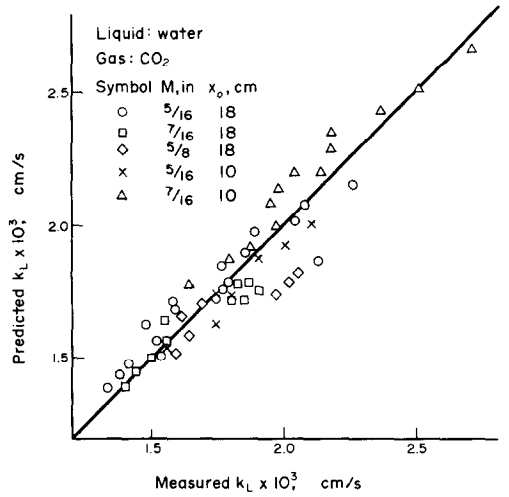

FIG. 5. Comparison of the results of the present model (with $C_{IMA} = 0.85$) with the data of Fortescue and Pearson [3, 10].

4.2.2. *Jet flows.* Davies and coworkers have investigated the turbulent mass-transfer characteristics of both water [11, 12] and kerosene [13, 14] jets. They employed the basic Levich postulate that the "dynamic thrust" of an eddy at the free interface is balanced by the excess surface pressure associated with the deformation of the surface by the eddy:

$$\rho V_0^2 = \frac{2\sigma}{R}. \tag{13}$$

It is interesting that even though Davies and Hameed [13, 19] point out that R increases rapidly downstream of the nozzle opening and reaches a value at the test section exit about 10 times that in the vicinity of the nozzle, they still take V_0 to be constant and equal to the shear velocity, V_*, within the nozzle. From the measurements of Davies [19], $R \propto t^{1/2}$, so from equation (13), the local $V_0 \propto t^{-1/4}$. For the Levich theory, the mass-transfer prediction based on these local values of V_0, $k_L \propto Re^{3/8}$, is in significant disagreement with the experimental data, which are described by $k_L \propto Re^{1.3}$.

In the present analysis, a characterization of the turbulence structure in the jet is provided by employing the same turbulence concepts which have described the fluid mechanics for flow downstream of a grid. The decay first follows the law of the "initial period", while for larger distances downstream, the energy decreases more rapidly and ultimately obeys the law of the "final period". A relatively short transition region separates these two periods of decay. The rate of decrease of kinetic energy during the initial period is given by:

$$\frac{dV^2}{dt} \cong -\frac{V^3}{L}. \tag{14}$$

The time scale for the energy decay, then, is

$$\frac{V^2}{\left|\frac{dV^2}{dt}\right|} \cong \frac{L}{V} \cong T \tag{15}$$

which shows that the length of duration of the initial period, t^*, is of the order of a few characteristic times of the energy-containing eddies. This order-of-magnitude analysis is substantiated by the experimental data of Batchelor and Townsend [20] and Batchelor [6] for flow downstream of a grid. These data indicate that $5\,T \lesssim t^* \lesssim 15\,T$, where T is the characteristic eddy time during the early stages of decay. A median value of $t^* = 10\,T$ is utilized here.

The jet is taken to move in the positive x-direction with the bulk velocity, $\bar{V}$. The initial period of decay is characterized by

$$V^{-2} = C_1(t - t_1) \text{ and } \lambda^2 = 10\nu(t - t_1) \tag{16}$$

where $t = x/\bar{V}$, t_1 and C_1 are constants, and λ, the microscale (or dissipation length scale) of turbulence, may be related to properties of the energy-containing motions by

$$\frac{\lambda^2}{L^2} = \frac{10}{Re_t}. \tag{17}$$

The constants are determined by requiring continuity of L and V at $x = 0$ to yield,

$$V = V(x=0)\left\{1 + \frac{V(x=0)}{L(x=0)}t\right\}^{-1/2} \tag{18}$$

$$L = L(x=0)\left\{1 + \frac{V(x=0)}{L(x=0)}t\right\}^{1/2}. \tag{19}$$

The $L(x=0)$ and $V(x=0)$ were evaluated from: $L(x=0) \cong 0.03d$ and $V(x=0) \cong V_*$ as before. For the purposes of the mass-transfer calculations, the intermediate region between the initial and final decay periods will be neglected. The final period of decay will be treated as beginning at $x = x^* = 10\bar{V}L(x=0)/V(x=0)$. It is characterized by

$$V^{-2} = C_2(t - t_2)^{5/2} \text{ and } \lambda^2 = 4\nu(t - t_2) \tag{20}$$

where C_2 and t_2 are constants. It can be shown that for the final period, $\lambda = \sqrt{(2/\pi)}L$. The constants C_2 and t_2 are determined by requiring continuity of L and V at $x = x^*$. The results are:

$$V = \frac{V(x^*)L(x^*)^{5/2}}{(2\pi\nu)^{5/4}} \frac{\bar{V}^{5/4}}{\left[x - x^* + \frac{L(x^*)^2\bar{V}}{2\pi\nu}\right]^{5/4}} \tag{21}$$

$$L = \left(\frac{2\pi\nu}{\bar{V}}\right)^{1/2}\left[x - x^* + \frac{L(x^*)^2\bar{V}}{2\pi\nu}\right]^{1/2}. \tag{22}$$

From equations (18)–(22), the range of Re_t for the

conditions employed by Davies and Ting is found to be 3.9–37, indicating that the large-scale motions dominate the mass-transfer process. The average mass-transfer coefficient is given by

$$k_L = \frac{2^{1/4} C_{\mathrm{IMA}}}{(c_s - c_b) t_{\exp}} \left\{ \int_0^{t^*} \tfrac{1}{2}[j_I(t;\beta=1) + j_I(t;\beta=-1)]\,\mathrm{d}t + \int_{t^*}^{t_{\exp}} \tfrac{1}{2}[j_F(t;\beta=1) + j_F(t;\beta=-1)]\,\mathrm{d}t \right\} \quad (23)$$

The stagnation-flow absorption fluxes for the initial period, j_I, and final period, j_F, are given in Appendix D.

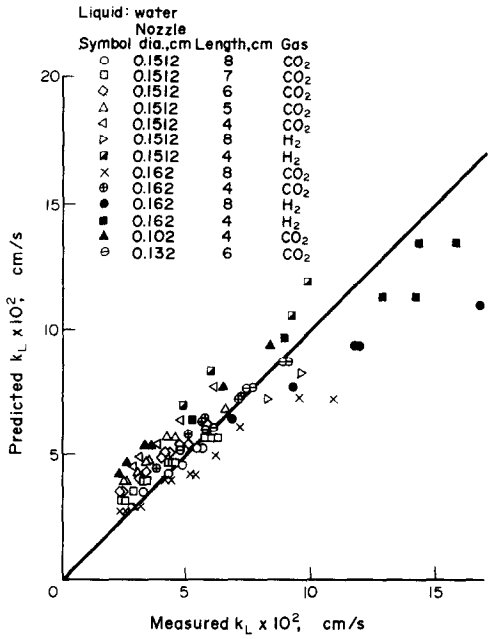

FIG. 6. Comparison of the results of the present model (with $C_{\mathrm{IMA}} = 0.50$) with the data of Davies and Ting [11, 12].

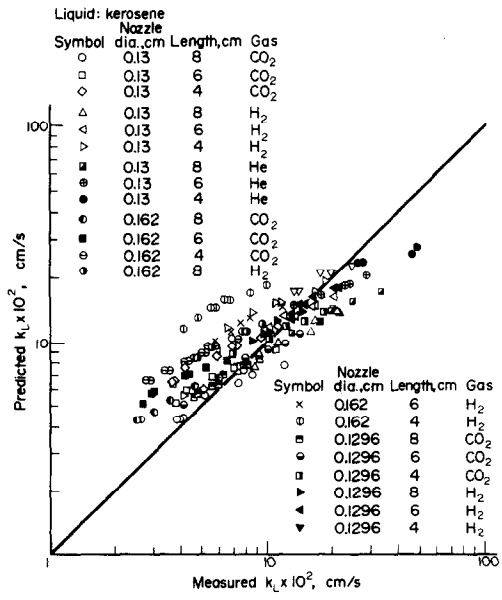

FIG. 7. Comparison of the results of the present model (with $C_{\mathrm{IMA}} = 0.66$) with the data of Davies and Hameed [13, 14].

For the water data, the best value of the constant, C_{IMA}, was found to be 0.50 with an average error of 26% and a sensitivity parameter of 0.58. The calculated k_L's based on the present model are compared with the experimental results in Fig. 6. The calculated results were found to be insensitive to the location of x^*, which separates the initial and final periods of decay. For example, calculations with $x^* = \bar{V}L(x=0)/V(x=0)$ gave somewhat lower k_L values, but with virtually no change in the sensitivity. Transient effects contributed up to 13% of the total absorption.

For the experimental conditions of Davies and Hameed, who used kerosene ($\sigma \sim 30$ dyn/cm), Re_t was 1.8–20; hence, the IMA also applies here. On following the same procedures employed with the water jet data, the best value for C_{IMA} was 0.66 with an average error of 41% and a sensitivity parameter of 0.51. The calculated k_L's are compared with the experimental results in Fig. 7. Transient contributions amounted up to 17% of the steady-state values.

4.3. *Comparisons of present and previous models*

Predictions from the Levich model, the large-eddy model, and the small-eddy model are compared with the results of the present model in Table 1 for the five sets of data from widely-differing flow systems. In order to compare models on the same basis, the least-squares values of the constants C_L, C_{LE} and C_{SE} are presented together with the average percent error, E, and the sensitivity parameter, S, for each data set. The constants C_L, C_{LE} and C_{SE} given in the first column of this table are those suggested by the original authors. The choice of the "appropriate" turbulence properties for each one of the models involves several suppositions, especially for cases that are quite different from those for which the models were originally constructed.

(a) Levich's model was originally presented for thin, vertical, falling, liquid films. The characteristic velocity, V_0, was identified with the shear velocity, V_*. Next, Davies and Ting made the same choice, but with V_* calculated at the exit of the nozzle. A more consistent choice would have been $V_0(t) = V(t)$, since $V_0(t=0) = V_* \approx V(t=0)$. This choice is also made for the grid-produced turbulence of Fortescue and Pearson. For the bubble (pipe) data of Lamont and Scott, it turns out that this same choice is also in agreement with the original specification, since $V_* \cong V$ for the core region. The same is also approximately true for Brown's experiment, since $V_* \cong V$ near the free interface.

(b) For the small-eddy model, the key question is whether to use local or total dissipation. The originators of the model applied it in terms of total dissipation [4]. For the largely non-uniform viscous-dissipation distribution in turbulent shear flows, this is not representative of the processes near the important interfacial region. An estimate of local dissipation is possible through equation (2). Such an estimate is considered preferable and is applied to the data of Brown and Lamont and Scott. For decaying turbulence, the estimate of dissipation based on $\varepsilon \simeq V^3/L$ is not accurate in the final period (due to the continual

narrowing of the overall wave number range which leads to viscous effects predominating the decay). Thus, a local dissipation estimated from the decrease of the kinetic energy of turbulence (as prescribed from the decay laws) is utilized.

By proceeding across a row corresponding to a given model in Table 1, one may assess its ability to predict transfer rates for the different data sets. In particular, the variation in the value of the constant required to give the best fit is an essential characteristic of the model's validity—the smaller the variation in the constant, the more reliable is the model. Proceeding down a column for a given data set provides insight into the differences in predictive capability between the various models. For the data sets of Brown and Lamont and Scott, for which the turbulence properties are known, the present model provides the lowest average error and the best sensitivity to the experimental conditions. The values of C_{IMA} required to give the best fit are very consistent, varying only by 7% from the mean of 0.68. The results obtained for the data sets of Fortescue and Pearson and Davies and coworkers are limited by the accuracy with which the requisite turbulence parameters, L and V, can be estimated. In both cases, the theory of decaying, homogeneous turbulence cannot be expected to provide more than an order-of-magnitude estimate for these parameters. Even so, the values of C_{IMA} are "consistent" with those from the previous data sets with known properties, and the average error and sensitivity obtained are acceptable. As might be expected, the large-eddy model does a good job in "predicting" the data of Fortescue and Pearson. Even in this case, however, the present model achieves a finite improvement, since by taking into account transient absorption, the constant comes more in line with values determined from other data sets, and a better sensitivity is achieved. Furthermore, it is not quite clear whether the decaying turbulent field of Fortescue and Pearson was completely free of shear-generated turbulence augmentation near the interface originating from the bottom of the relatively thin stream. Such an effect, if present, would explain the somewhat larger-than-expected estimated value of C_{IMA} for these data.

Davies and Hameed [13] concluded that the damping of the bulk turbulence in the liquid jets was due primarily to surface tension forces rather than bulk viscous forces. However, calculations based on equation (13) and the measured [19] variation of R show that viscosity should be more effective in damping the bulk turbulence [21]. This conclusion is also supported by the consistency of the liquid-jet mass-transfer predictions summarized in Table 1 for the present model. In addition, mass-transfer predictions based on the Levich model with $V_0(t) = V(t)$ (which characterizes the viscous damping of the bulk turbulence) are far superior to those based on $V_0 = V_*$ (as assumed by Davies and coworkers) and $V_0(t) \propto t^{-1/4}$ [as indicated from equation (13) and the measured variation of R].

Since the turbulence properties L and V were not measured for the open-channel flow of Bieber [22, 23], mass-transfer predictions for the small-eddy model (with $\varepsilon = V^3/L$) the large-eddy model, and the present model could not be carried out. Calculations for the Levich model with $V_0 = V_*$ give $C_L = 7.6$, $E = 18\%$, and $S = 1.2$. This value of C_L is in marked disagreement with the C_L value of 1.6 deduced from the open-channel data of Brown.

5. ASSESSMENT OF SURFACE TENSION EFFECTS

If surface tension is considered to be an important variable in the mass-transfer process, dimensional analysis indicates that

$$Sh = \frac{k_L L}{D} = f(Sc, Re_t, We_t) \tag{24}$$

where an additional dimensionless group, the turbulence Weber number, $We_t = V\sqrt{(\rho L/\sigma)}$, also appears. Here, the steady-state mass-transfer process is considered for simplicity. As before, we have:

$$k_L = f(Re_t, We_t)\frac{(Dv)^{1/2}}{L} \tag{25}$$

where f is an unknown function. For the time being, let us suppose that $f(Re_t, We_t) \simeq g(Re_t)h(We_t)$, which is a functional form widely used in empirical modelling. We then obtain:

$$k_L = h(We_t)g(Re_t)\frac{(Dv)^{1/2}}{L}. \tag{26}$$

If it is assumed, as indicated by the previous developments, that $g(Re_t) \simeq C_1 Re_t^{1/2}$ for $Re_t \lesssim Re_t^*$ and $g(Re_t) \simeq C_2 Re_t^{3/4}$ for $Re_t \gtrsim Re_t^*$, where C_1 and C_2 are constants, we have

$$k_L = \begin{cases} k_L^I = C_1 h(We_t)\left(\dfrac{DV}{L}\right)^{1/2} \text{ for } Re_t \lesssim Re_t^* & (27) \\ k_L^D = C_2 h(We_t) D^{1/2}\left\{\dfrac{V^3}{\nu L}\right\}^{1/4} \text{ for } Re_t \gtrsim Re_t^*. & (28) \end{cases}$$

Comparison of equation (27) with equation (9) and equation (28) with equation (7) indicates that

$$C_{\mathrm{IMA}} \sim C_1 h(We_t) \text{ and } C_{\mathrm{UET}} \sim C_2 h(We_t). \tag{29}$$

These equations demonstrate that the constants C_{IMA} and C_{UET} are functions of surface tension, but only as it occurs in the dimensionless group, We_t. For the calculations presented in the previous section, the range of We_t extends over three orders of magnitude, with negligible variation in the deduced values of C_{IMA}. This indicates that C_{IMA} is only a weak function of surface tension. A comparison of the ranges of Re_t and We_t for the experiments is given in Table 5. It is probable that the dependence of C_{UET} on σ is also very slight. However, the range of We_t encountered in Brown's experiments covers only about one order of magnitude, so a more precise determination of the nature of the dependency of C_{UET} on We_t must await further experimental and/or theoretical results. An hypothesis, formulated from the above considerations, may be stated as: for turbulent flows in which the

Table 5. Ranges of turbulence Reynolds and Weber numbers

Data set	Re_t Range	We_t Range
Open-channel flow, Brown [7]	128–3940	0.13–1.48
Bubble flow, Lamont and Scott [4, 8, 9]	4.3–38	0.024–0.29
Grid-produced turbulence Open-channel flow, Fortescue and Pearson [3, 10]	2.3–113	0.0032–0.20
Jet flows: water, Davies and Ting [11, 12]	3.9–37	0.025–0.59
kerosene, Davies and Hameed [13, 14]	1.8–20	0.026–0.92

inertial motions control the mass transfer, k_L should be independent of σ (at least for $0.001 \lesssim We_t \lesssim 1$) and depend only on the "bulk" turbulence properties, L and V, in the manner specified by equation (9).

6. CONCLUSIONS

A turbulence-centered model appears capable of describing mass transfer rates at gas–liquid interfaces found in open-channel flows, bubble (pipe) flows, jet flows, and film flows. Surface tension effects are not likely to dominate the process. Yet, it would be desirable to incorporate corrections for such effects in the present model. Additional mass-transfer data covering wider ranges of surface tension and turbulence Reynolds number are needed for this purpose. Such data in the high turbulence Reynolds number range (more than a few hundred) are also needed to explore further the existence of the two mass-transfer regimes proposed here. This concept is presently fully supported by the data of Brown, which comprise the only applicable experimental information available.

Acknowledgements—This work has been supported by: a Faculty Assistance Grant from E. I. duPont deNemours & Co. (TGT), the NSF GK-36488 Grant from the National Science Foundation (TGT and RNH) and a David Ross Fellowship from the Purdue Research Foundation (LKB).

REFERENCES

1. L. K. Brumfield, R. N. Houze and T. G. Theofanous, Turbulent mass transfer at free, gas–liquid interfaces, with applications to film flows, *Int. J. Heat Mass Transfer* **18**, 1077–1081 (1975).
2. V. G. Levich, Theory of the diffusion kinetics of heterogeneous chemical process, Part III, *Zh. Fiz. Khim.* **22**, 721–729 (1948); V. G. Levich, *Physiocochemical Hydrodynamics*. Prentice-Hall, Englewood Cliffs, N.J. (1962).
3. G. E. Fortescue and J. R. A. Pearson, On gas absorption into a turbulent liquid, *Chem. Engng Sci.* **22**, 1163–1176 (1967).
4. J. C. Lamont and D. S. Scott, An eddy cell model of mass transfer into the surface of a turbulent liquid, *A.I.Ch.E. Jl* **16**, 513–519 (1970).
5. J. O. Hinze, *Turbulence*. McGraw-Hill, New York (1959).
6. G. K. Batchelor, *The Theory of Homogeneous Turbulence*. Cambridge University Press, London (1967).
7. L. C. Brown, Oxygen transfer in open channel flow, Ph.D. thesis, University of Wisconsin (1970).
8. J. C. Lamont, Gas absorption in cocurrent turbulent bubble flow, Ph.D. thesis, University of British Columbia (1966).
9. J. C. Lamont and D. S. Scott, Mass transfer from bubbles in cocurrent flow, *Can. J. Chem. Engng* **44**, 201–208 (1966).
10. G. E. Fortescue, Mass transfer into turbulent liquids, Ph.D. thesis, University of Cambridge (1965).
11. J. T. Davies and S. T. Ting, Mass transfer into turbulent jets, *Chem. Engng Sci.* **22**, 1539–1548 (1967).
12. S. T. Ting, Gas absorption and eddies, Ph.D. thesis, University of Birmingham (1967).
13. J. T. Davies and A. Hameed, Gas absorption into turbulent jets of kerosene, *Chem. Engng Sci.* **26**, 1295–1296 (1971).
14. A. Hameed, Hydrodynamic and mass transfer properties of surfaces, Ph.D. thesis, University of Birmingham (1969).
15. G. Q. Martin and L. N. Johanson, Turbulence characteristics of liquids in pipe flow, *A.I.Ch.E. Jl* **11**, 29–33 (1965).
16. W. T. Pennell, E. M. Sparrow and E. R. G. Eckert, Turbulence intensity and time-mean velocity distributions in low Reynolds number turbulent pipe flows, *Int. J. Heat Mass Transfer* **15**, 1067–1074 (1972).
17. F. N. Peebles and H. J. Garber, Studies on the motion of gas bubbles in liquids, *Chem. Engng Prog.* **49**, 88–97 (1953).
18. J. L. L. Baker and B. T. Chao, An experimental investigation of air bubble motion in a turbulent water stream, *A.I.Ch.E. Jl* **11**, 268–273 (1965).
19. J. T. Davies, *Turbulence Phenomena*. Academic Press, New York (1972).
20. G. K. Batchelor and A. A. Townsend, Decay of isotropic turbulence in the initial period, *Proc. R. Soc.* **193A**, 539–558 (1948).
21. L. K. Brumfield and T. G. Theofanous, Turbulent mass transfer in jet flow and bubble flow—application of the Levich theory, Submitted for publication.
22. A. G. Bieber, Absorption of a gas into a liquid in turbulent open channel flow, Ph.D. thesis, Virginia Polytechnic Institute and State University (1971).
23. B. D. Prasher, Gas absorption into a turbulent liquid, *Chem. Engng Sci.* **28**, 1230–1232 (1973).
24. L. K. Brumfield, On predicting mass transfer at turbulent, free interfaces with a large eddy model, M.S. thesis, Purdue University (1971).
25. J. T. Davies, Turbulence phenomena at free surfaces, *A.I.Ch.E. Jl* **18**, 169–173 (1972).

APPENDIX A

Unsteady Mass Transfer in Eddy Models (with Constant Length and Velocity Scales)

Unsteady mass transfer into the large eddy is analyzed by taking the velocity field to be that of the Fortescue–Pearson [3] roll cell. At time $t = 0$, the eddy is exposed and participates in the mass transfer process until time $t = t_{exp}$. The mathematical problem to be solved, then, is

$$\frac{\partial c}{\partial t} + V_m \sin\frac{\pi x}{L}\frac{\partial c}{\partial x} - \frac{\pi V_m y}{L}\cos\frac{\pi x}{L}\frac{\partial c}{\partial y} = D\frac{\partial^2 c}{\partial y^2}, \quad \begin{matrix} 0 < x < L \\ 0 < y < \infty \\ t > 0 \end{matrix} \tag{A.1}$$

$$c = c_b \text{ at } t = 0$$

$$c = c_b \text{ at } y \to \infty$$

$$c = c_s \text{ at } y = 0, \quad t > 0.$$

A solution of the form $c = c(\eta)$, where $\eta = \dfrac{y}{\delta(x, t)}$, is sought:

$$-c'\eta\xi = Dc'' \tag{A.2}$$

and

$$\frac{1}{2}\frac{\partial(\delta^2)}{\partial t} + \frac{V_m}{2}\sin\frac{\pi x}{L}\frac{\partial(\delta^2)}{\delta x} + \frac{\pi V_m}{L}\cos\frac{\pi x}{L}\delta^2 = \xi \tag{A.3}$$

where ξ is an arbitrary constant. Equation (A.2) is solved using the boundary conditions

$$c = c_s \text{ for } \eta = 0 \text{ and } c = c_b \text{ for } \eta \to \infty.$$

Equation (A.3) is solved using the condition

$$\delta = 0 \text{ at } t = 0 \text{ for all } x.$$

The result is:

$$\frac{c-c_b}{c_s-c_b} = \operatorname{erfc}\left\{\frac{y}{2}\sqrt{\left(\frac{\pi V_m}{DL}\left[\coth\left(\frac{\pi V_m t}{L}\right)+\cos\left(\frac{\pi x}{L}\right)\right]\right)}\right\}. \quad \text{(A.4)}$$

The average mass-transfer coefficient, k_L, is

$$k_L = 1.07F(\alpha)\left(\frac{DV}{L}\right)^{1/2} \quad \text{(A.5)}$$

where

$$F(\alpha) \equiv \frac{\pi}{2(\sqrt{2})\alpha}\int_0^{\alpha}\int_0^{1}\sqrt{(\coth \pi t' + \cos \pi x')}\,dx'\,dt' \quad \text{(A.6)}$$

and $$\alpha = \frac{t_{\exp}}{T}, \quad T = \frac{L}{V_m}, \quad \text{and} \quad V_m = (\sqrt{2})V. \quad \text{(A.7)}$$

The function $F(\alpha)$ is plotted in Fig. 1. For $\alpha \geqslant 0.85$, $F(\alpha) = 1 + (0.44/\alpha)$.

APPENDIX B

Unsteady Mass Transfer in Eddy Models (with Arbitrary, Time-Varying Length and Velocity Scales)

It has been pointed out [24] that for a number of modifications stemming from the convective-diffusion equation for the roll cell, the local steady-state absorption flux across the surface of the eddy is approximately linear, having a maximum at the forward stagnation flow ($x = 0$) and a minimum at the reverse stagnation flow ($x = L$). The approximation of lincarity is even more exact for unsteady absorption. The mass transfer analysis for an eddy with a time-varying length (L) and velocity (V) scale becomes mathematically tractable, then, by considering only the stagnation regions.

At a stagnation flow, equation (A.1) becomes

$$\frac{\partial c}{\partial t} - \frac{\pi\beta y}{T(t)}\frac{\partial c}{\partial y} = D\frac{\partial^2 c}{\partial y^2} \quad \text{(B.1)}$$

where $\beta \equiv 1$ when $x = 0$ and $\beta \equiv -1$ when $x = L$, and $T(t) = L(t)/V_m(t)$. $T(t)$ is the characteristic eddy time and is an arbitrary function of time. The initial and boundary conditions are as specified in equation (A.1). Equation (B.1) may be solved by the same similarity-solution technique of Appendix A to yield the local, time-dependent absorption flux

$$j(t;\beta) = (c_s - c_b)\left\{\frac{D\exp\left[2\pi\beta\int_0^t \frac{dt'}{T(t')}\right]}{\pi\int_0^t \exp\left[2\pi\beta\int_0^{t'}\frac{dt''}{T(t'')}\right]dt'}\right\}^{1/2}. \quad \text{(B.2)}$$

The area-averaged flux for the eddy is denoted by $j'(t)$ and is given by

$$j'(t) = \tfrac{1}{2}[j(t;\beta = 1) + j(t;\beta = -1)]. \quad \text{(B.3)}$$

An estimate of k_L based on this approximation is denoted by k'_L and is

$$k'_L = \frac{1}{(c_s - c_b)t_{\exp}}\int_0^{t_{\exp}} j'(t)\,dt. \quad \text{(B.4)}$$

For the case where T is independent of time, k'_L is calculated from equation (B.4) to be

$$k'_L = 2^{-1/4}G(\alpha)\left(\frac{DV}{L}\right)^{1/2} \quad \text{(B.5)}$$

where

$$G(\alpha) \equiv \frac{1}{\alpha}\int_0^{\alpha}\{[1-\exp(-2\pi\eta)]^{-1/2} + [\exp(2\pi\eta)-1]^{-1/2}\}\,d\eta. \quad \text{(B.6)}$$

For finite α, $G(\alpha) \approx F(\alpha)$ ($F(\alpha)$ differs from $G(\alpha)$ by less than 16%, for example, for $\alpha \geqslant 1$) and as $\alpha \to \infty$, $G(\alpha) \to F(\alpha) \to 1$.

APPENDIX C

Derivation of Mass-Transfer Expressions for Decaying Turbulent Flow Downstream of a Grid

The turbulence properties downstream of a grid vary with position as [3]

$$V = 0.086V_S\left(\frac{M}{x-10M}\right)^{1/2} \quad \text{(C.1)}$$

$$L = \left[\frac{M(16M+x)}{160}\right]^{1/2} \quad \text{(C.2)}$$

where V_S, the surface velocity, is the velocity with which the turbulence structure is convected down the channel, x is the distance downstream of the grid, and M is the mesh size. For the absorption process,

$$x = x_0 + V_S t \quad \text{(C.3)}$$

where x_0 is the distance upstream of the test section entrance at which the grid is located. From these three equations, $V(t)$ and $L(t)$ are obtained. Now $j(t;\beta)$, as calculated from equation (B.2), is

$$j(t;\beta) = (c_s - c_b) \times \left\{\frac{D[2(t^2+bt+a)^{1/2}+2t+b]^{2\beta c}}{\pi\int_0^t [2(\eta^2+b\eta+a)^{1/2}+2\eta+b]^{2\beta c}\,d\eta}\right\}^{1/2} \quad \text{(C.4)}$$

where a, b and c are defined by

$$a = \frac{(x_0-10M)(x_0+16M)}{V_s^2}$$

$$b = \frac{2x_0+6M}{V_s}$$

$$c = 0.086(320)^{1/2}\pi.$$

APPENDIX D

Derivation of Mass-Transfer Expressions for Turbulent Liquid Jet Flow

The turbulence properties vary along the length of the jet as shown in equations (18), (19), (21), and (22). These expressions, in conjunction with equation (B.2), yield the stagnation flow mass fluxes, $j_I(t;\beta)$ and $j_F(t;\beta)$, for the initial and final period, respectively.

$$j_I(t;\beta) = (c_s - c_b) \times \left\{\frac{DV(x=0)[2(\sqrt{2})\pi\beta+1]\left[1+\frac{V(x=0)}{L(x=0)}t\right]^{2(\sqrt{2})\pi\beta}}{\pi L(x=0)\left[\left(1+\frac{V(x=0)}{L(x=0)}t\right)^{2(\sqrt{2})\pi\beta+1}-1\right]}\right\}^{1/2} \quad \text{(D.1)}$$

$$j_F(t;\beta) = (c_s - c_b) \times \left\{\frac{(D/\pi)\exp[-\beta q_1(t+q_2)^{-3/4}]}{C_2 + \int_{t^*}^t \exp[-\beta q_1(t'+q_2)^{-3/4}]\,dt'}\right\}^{1/2} \quad \text{(D.2)}$$

where

$$q_1 = \frac{8(\sqrt{2})\pi V(t^*)L(t^*)^{5/2}}{3(2\pi\nu)^{7/4}}$$

$$q_2 = \frac{L(t^*)^2}{2\pi\nu} - t^*$$

$$q_3 = 1 + \frac{V(x=0)}{L(x=0)} - t^*$$

$$q_4 = \frac{4(\sqrt{2})V(t^*)L(t^*)}{3\nu}$$

$$C_2 = \frac{L(x=0)(q_3^{2(\sqrt{2})\pi\beta+1}-1)}{V(x=0)[2(\sqrt{2})\pi\beta+1]q_3^{2(\sqrt{2})\pi\beta}\exp(\beta q_4)}.$$

TRANSFERT DE MASSE TURBULENT A L'INTERFACE LIBRE LIQUIDE-GAZ, ET APPLICATION AU CAS D'UN CANAL DECOUVERT, DES ECOULEMENTS DE BULLES ET DES JETS

Résumé—On discute l'absorption d'un gaz par un liquide turbulent en l'absence de cisaillement interfacial (imposé par le gaz). Le principal outil utilisé est l'analyse dimensionnelle. Deux régimes distincts de transfert de masse ont été identifiés, associés aux évolutions turbulentes des tourbillons porteurs d'énergie et des tourbillons siège de la dissipation. On a obtenu des relations pour chacun des régimes et un critère basé sur le nombre de Reynolds de turbulence permet de déterminer le domaine d'application de chaque relation. Le modèle de transfert de masse est appliqué à quatre configurations d'écoulements pour lesquelles ou bien les données turbulentes sont disponibles, ou bien elles peuvent être estimées (écoulement en canal découvert avec ou sans turbulence de grille initiale, écoulement de bulles, jet turbulent).

TURBULENTER STOFFAUSTAUSCH AN FREIEN GAS-FLÜSSIGKEITS-GRENZFLÄCHEN IN BEZUG AUF DIE ANWENDUNG IN OFFENEN KANÄLEN, BEI BLASENSTRÖMUNG UND AN STRAHLEN

Zusammenfassung—Die Absorption von Gasen in einer turbulenten Flüssigkeit bei Abwesenheit äußerer (durch das Gas aufgezwungener) Grenzflächenschubspannungen wird diskutiert. Es werden zwei Regime des Stoffaustausches unterschieden, nämlich solche mit energieerhaltenden und solche mit energiedissipierenden turbulenten Strömungen. Es werden Beziehungen für beide Regime angegeben, ebenso ein Kriterium für die Abgrenzung, das auf der turbulenten *Re*-Zahl beruht. Das Stoffaustauschmodell wird für vier Strömungsfälle ausgewertet, für welche Turbulenzdaten entweder vorhanden oder abgeschätzt werden können (Strömung im offenen Kanal mit und ohne Turbulenzgittern, Blasenströmung und Strahlströmung).

ТУРБУЛЕНТНЫЙ ПЕРЕНОС МАССЫ НА СВОБОДНОЙ ПОВЕРХНОСТИ РАЗДЕЛА МЕЖДУ ГАЗОМ И ЖИДКОСТЬЮ ПРИМЕНИТЕЛЬНО К ТЕЧЕНИЮ В ОТКРЫТОМ КАНАЛЕ, ПУЗЫРЬКОВОМУ И СТРУЙНОМУ ТЕЧЕНИЯМ

Аннотация — С помощью анализа размерностей рассматривается процесс абсорбции газа турбулентным потоком жидкости при отсутствии внешнего (вызываемого газом) касательного напряжения на границе раздела фаз. Выявлено два различных режима переноса массы при турбулентном течении с диссипацией и без диссипации энергии. Для каждого режима выведены соотношения и на основании турбулентного числа Рейнольдса определен критерий применимости данных отношений. Проверку модели переноса массы провели на четырех видах течения, для которых имеются или можно получить данные по турбулентности (течение в открытом канале при наличии и отсутствии турбулизирующих решеток, пузырьковое течение и струйное течение).